

# Tracing the W3/W4/W5 and Perseus complex dynamical evolution with star clusters

A. Della Croce<sup>1,2\*</sup>, E. Dalessandro<sup>2</sup>, E. Vesperini<sup>3</sup>, M. Bellazzini<sup>2</sup>, C. Fanelli<sup>2</sup>, L. Origlia<sup>2</sup>, and N. Sanna<sup>4</sup>

<sup>1</sup> Department of Physics and Astronomy 'Augusto Righi', University of Bologna, via Gobetti 93/2, I-40129 Bologna, Italy

<sup>2</sup> INAF – Astrophysics and Space Science Observatory of Bologna, via Gobetti 93/3, I-40129 Bologna, Italy

<sup>3</sup> Department of Astronomy, Indiana University, Swain West, 727 E. 3rd Street, IN 47405 Bloomington, USA

<sup>4</sup> INAF - Osservatorio Astrofisico di Arcetri, Largo Enrico Fermi 5, I-50125 Florence, Italy

Reporter : Zeng Guangya

# outline

- 1. Introduction
- 2. Identifying star clusters in the W345 region
- 3. Properties of star clusters in the W3/W4/W5 region
- 4. The kinematics of the Perseus complex
- 5. Summary and conclusions

# Introduction

# Introduction

- They focus on the W3/W4/W5 region (hereafter W345) of the Perseus complex. W345 is a wellstudied region of recent star formation, containing two giant H II regions (W4 and W5), a massive molecular ridge with active star formation (W3), and several embedded star clusters (Carpenter 2000; Koenig et al. 2008; Román-Zúñiga et al. 2015; Jose et al. 2016; Sung et al. 2017).
- In addition, they previously identified two major cluster aggregates within the Perseus complex, namely LISCA I (Dalessandro et al. 2021) and LISCA II (Della Croce et al. 2023).
- The LISCA systems and the W345 region lie within the Perseus: a large and massive complex located toward the Galactic anticenter (at about 2 – 3 kpc from the Sun), characterized by recent star formation and showing low dispersion in chemical element abundances (Fanelli et al. 2022a,b).
- This work aims to carefully characterize the star cluster population of the W345 region, and to use star cluster within the Perseus complex to trace its formation conditions and evolution.

# Identifying star clusters in the W345 region

- To study the stellar population of the W345 complex, they preliminary retrieved from the Gaia archive<sup>1</sup> sources with Galactic coordinates  $\ell \in [133.5^\circ; 138.5^\circ]$  and  $b \in [-0.3^\circ; 2^\circ]$ , having G magnitudes brighter than 18 and with parallax and proper motion (PM) measurements. The ranges are defined such that they enclose the W345 complex.
- They performed an unsupervised clustering analysis on the whole catalog using the HDBSCAN algorithm (McInnes et al. 2017) to identify overdensities in the five-dimensional space of Galactic coordinates ( $\ell$ ,  $b$ ), PM ( $\mu\alpha^*$ ,  $\mu\delta$ ), and parallax ( $\varpi$ ). Twelve overdensities were thus identified as star cluster candidates in the region, but four of them were then flagged as false detections by the post-processing routine.
- They then studied the parallax and PM distributions for the eight clusters identified. The observed parallax and PM distributions were deconvolved using Gaussian modeling and properly accounting for errors and correlations between measurements, thereby obtaining their intrinsic distributions.

- Figure 1 shows the parallax and PM intrinsic distributions. Five out of eight clusters presented compatible distributions in both spaces: IC 1848, IC 1805, Berkeley 65, UBC 420, and SAI 24. They then defined the sources belonging to the W345 region by selecting stars with parallax and PM within  $3\sigma$  from the mean value of any of the five clusters. The final catalog counts 8869 sources.

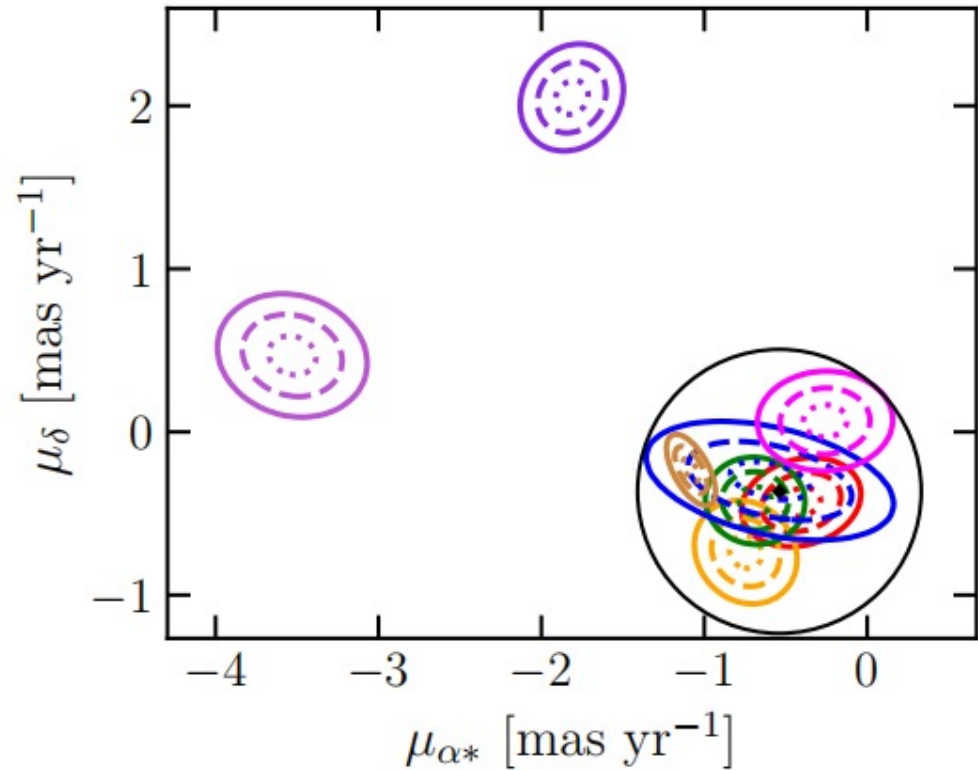
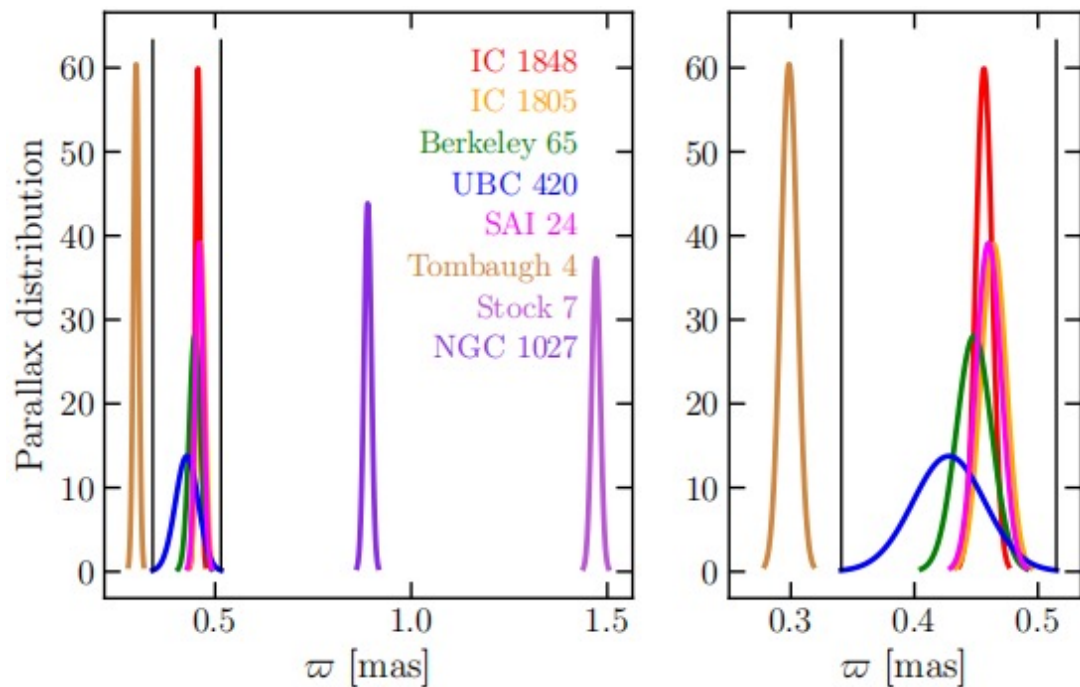


**Fig. 1.** Intrinsic, i.e. deconvolved, parallax (top panel), and PM (bottom panel) distributions for the eight clusters in the region defined by the preliminary Galactic coordinates ranges. Cluster names are reported in the top left panel. Black lines show the parallax and PM ranges adopted for selecting *Gaia* sources. The top right panel shows a narrower parallax range centered around the W345 star clusters to visualize the cluster parallax distributions better. Finally, in the bottom panel, different contours represent the 1 $\sigma$  (dotted lines), 2 $\sigma$  (dashed lines), and 3 $\sigma$  (solid lines) regions for each cluster. Also, correlations among  $\mu_{\alpha^*}$  and  $\mu_\delta$  are visible.

# **Properties of star clusters in the W3/W4/W5 region**

# Structure

- They constructed projected number counts density profiles for each cluster. They then fitted the observed density profiles with Plummer (1911) models. The Plummer radii ( $R_{\text{Plummer}}$ , inferred from the density profile fitting) and the 2D radii enclosing half of the members ( $R_{50}$ , directly computed from the cluster member spatial distributions) agree in general within less than  $1\sigma$ .
- They further characterized the morphological properties of each cluster by determining the axis ratio ( $q$ ) and the position angle (PA).

- Figure 4 presents the spatial distribution of cluster members with best-fit ellipses on top of false RGB images of the gas emission in the region. Generally, all clusters in their analysis are pretty elongated, with the youngest clusters representing the most extreme cases.

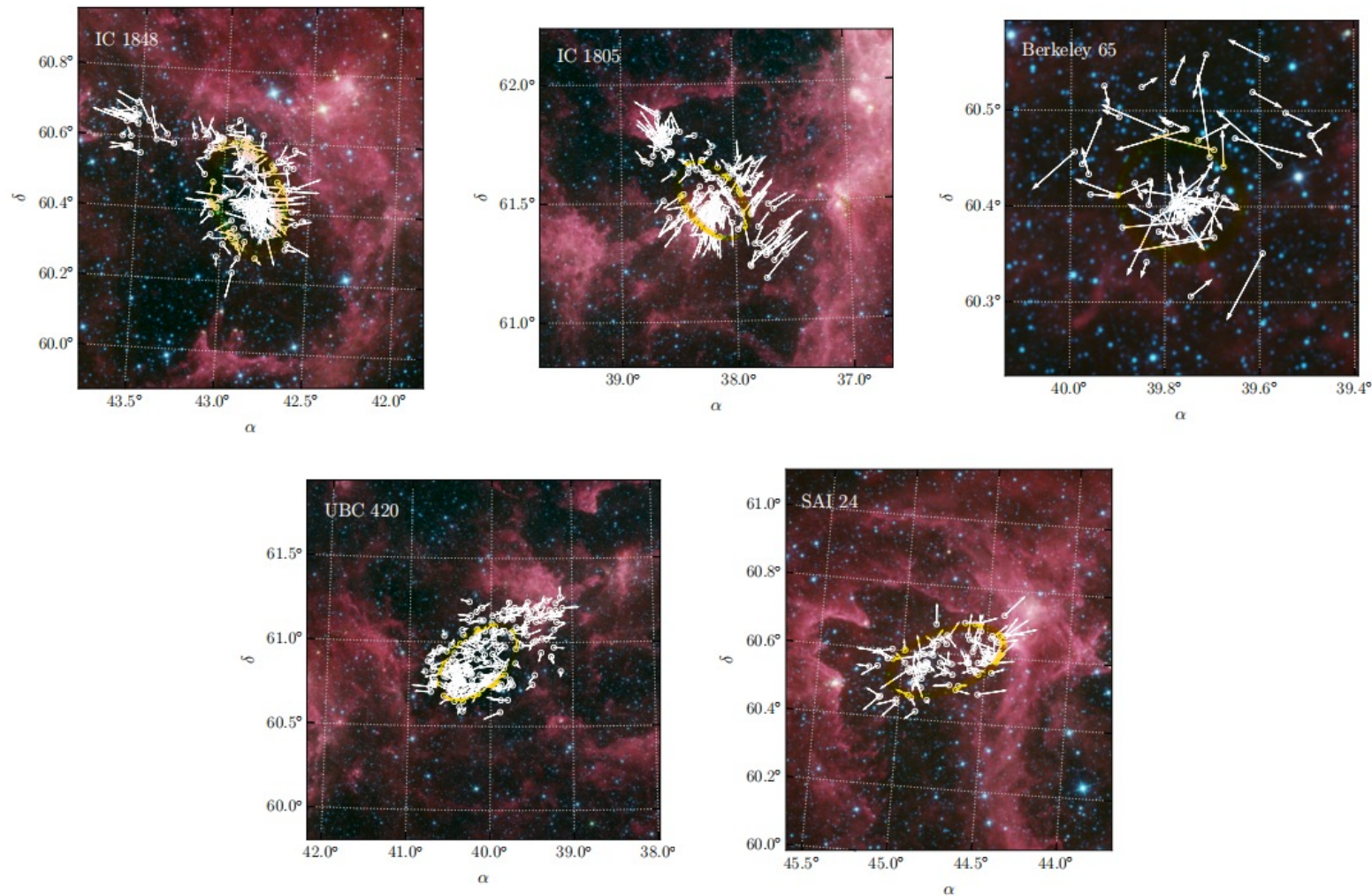


**Fig. 4.** On-sky spatial distribution of cluster members. For each cluster star, PM vectors are shown on top of the RGB image of the region from the allWISE survey. We mapped the W3 band in red, W2 in green, and W1 in blue. The W3 filter mainly traces small grain dust and polycyclic aromatic hydrocarbon emissions, whereas the W1 and W2 filters are dominated by young stars (Wright et al. 2010). The best-fit ellipses of the spatial distributions are shown in gold.

# Differential reddening and cluster ages

- They constrained cluster ages by fitting the cumulative luminosity function in the differential reddening corrected G band. Their sample were cross-matched with panSTARRS DR1. Then, for each star, they computed the distance along the reddening vector from the median colors of the closest 50 neighbors and a reference point (see Della Croce et al. 2023, for further technical details). Figure 5 shows the resulting two-dimensional reddening map of the region: as expected, sparser areas are characterized by higher extinction values, suggesting that lower-density regions correspond to areas of significant photometric incompleteness.

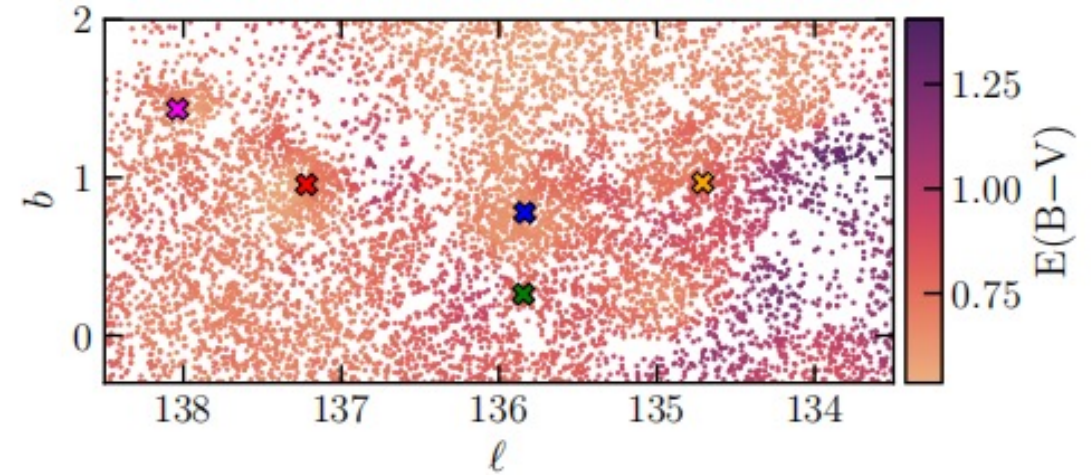


**Fig. 5.** Spatial distribution in Galactic coordinates of *Gaia* DR3 sources, selected according to Sect. 2. Each star is color-coded according to its reddening value. Crosses show the centers of the five stellar clusters analyzed in this work (SAI 24 in purple, IC 1848 in red, Berkeley 65 in green, UBC 420 in blue, and IC 1805 in yellow).

- Figure 6 shows the differential reddening corrected color-magnitude diagrams along with the best-fit isochrones. Their analysis shows that the clusters in the W345 region are almost coeval with Berkeley 65 being the older one and IC 1805, IC 1848, and SAI 24 are the youngest clusters in the region.

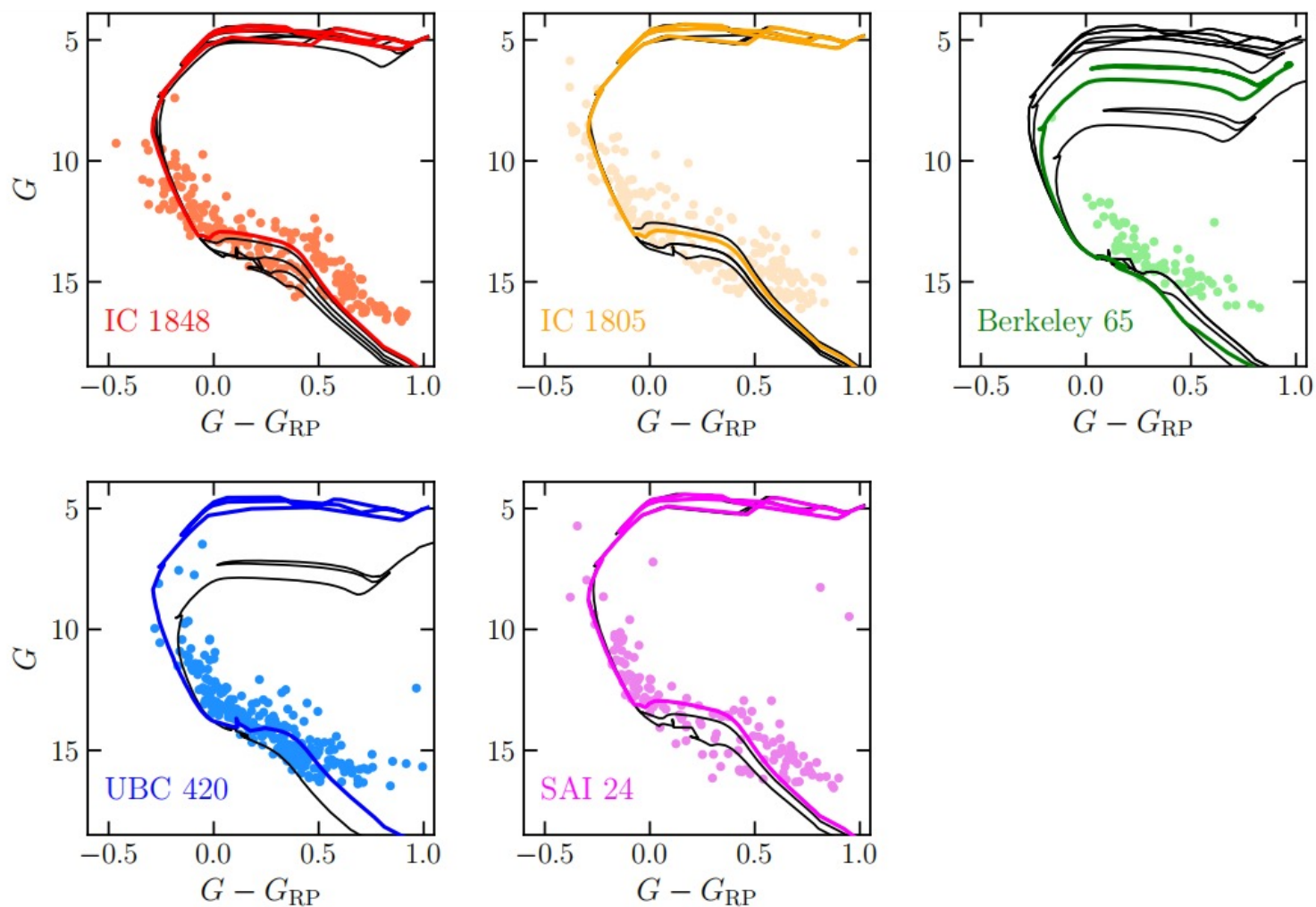


**Fig. 6.** Color magnitude diagrams in the *Gaia* filters for cluster members. The best-fit isochrones from differential-reddening-corrected, *G*-band luminosity function fits are shown using the same color palette as cluster members. In black are multiple isochrones from literature works: [Cantat-Gaudin et al. \(2020\)](#); [Dias et al. \(2021\)](#); [Hunt & Reffert \(2023\)](#); [Cavallo et al. \(2024\)](#).

# Kinematics

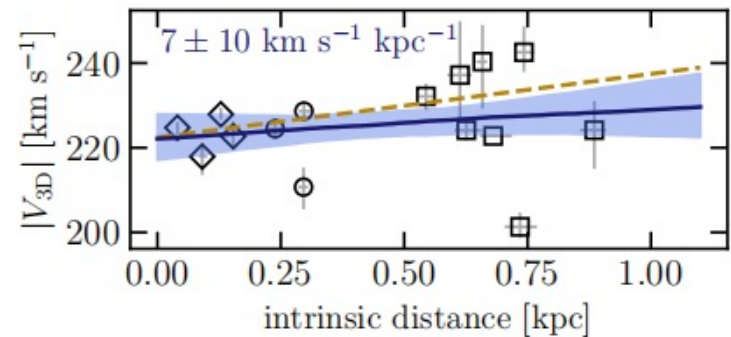
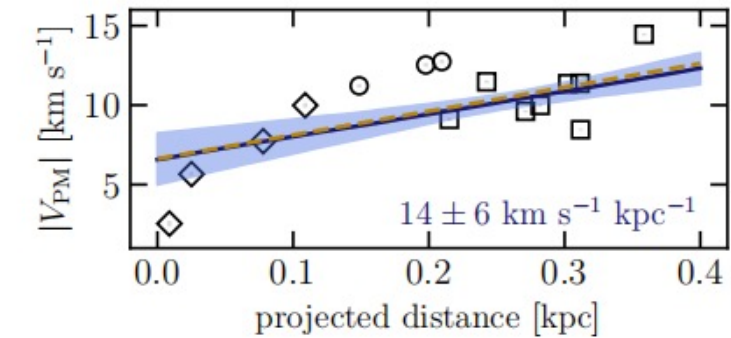
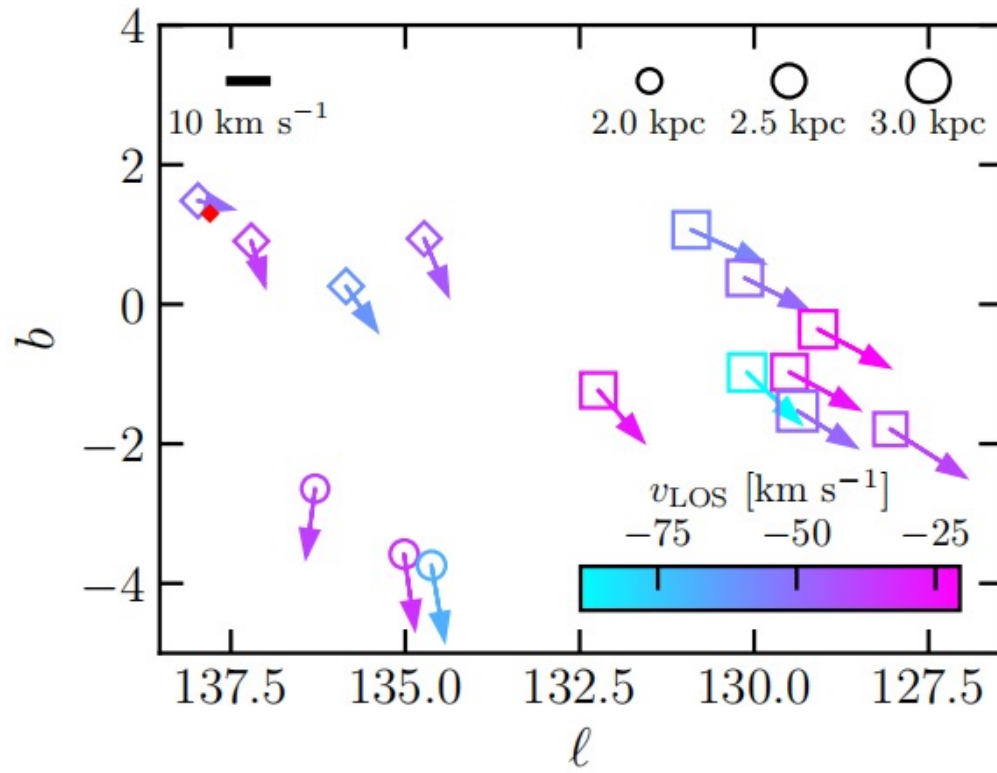
- In Fig. 4, at least three clusters exhibit clear expansion features i.e., IC 1848, IC 1805, and SAI 24. By investigating the distribution of individual radial velocities ( $v_R$ ), they found that while a fraction of stars is symmetrically distributed around zero within  $0.7 R_{50}$ , there is an excess of stars departing from the cluster center with increasing speed, hence driving the expansion signal also within  $R_{50}$ . Furthermore, most cluster members are enclosed within the tidal radius and there is no significant evidence of extra-tidal features. This suggests that internal processes are likely responsible for the observed expansion rather than Galactic tidal forces.
- In the case of expansion-driven elongations, they would expect tighter correlations between  $v_R$  and elliptical radii ( $R_{ell}$ ) than with circular radii. However, they did not find significant differences for all the clusters investigated except possibly for IC 1848. This suggests that the cluster's internal kinematics does not drive the present-day cluster morphologies. In contrast, it is likely inherited either from processes that occurred earlier (possibly tidal interactions or mergers) or from the parent gas structure.

# **The kinematics of the Perseus complex**

# 3D cluster positions and velocities

- They constructed a catalog of star clusters in the Perseus complex by gathering the star clusters of the W345 region determined in this paper (see Sect. 3), in LISCA I (Dalessandro et al. 2021), and LISCA II (Della Croce et al. 2023). They obtained mean sky positions, PM components, and distances for all clusters directly from their members, and acquired the line-of-sight velocity ( $v_{\text{LOS}}$ ) components by merging multiple catalogs.

- Figure 10 shows the absolute, on-sky velocities for the star clusters in the Perseus complex. Román-Zúñiga et al. (2019) found a Hubble-like expansion pattern for the region using individual stars. The projected star cluster kinematics qualitatively fits into this picture (see the top-right panel in Fig. 10). However, considering the 3D cluster positions and velocities in the Galaxy, this large-scale motion is not observed. They found no net trend with the intrinsic distance (see the bottom-right panel of Fig. 10). This may be because the Perseus complex spans more than 1 kpc along the LOS, hence when looking at the PM only they are projecting an almost 1.2 kpc-deep on a  $10^\circ$ -wide region.



# The projected kinematics

- Figure 11 presents the top-down view of the Galactic disk for the Perseus region. Interestingly, star clusters appear to be moving almost parallel to the arm. This, together with the Fig. 10 discussion, argues in favor of the Hubble-like expansion flow reported by Román-Zúñiga et al. (2019) likely being a projection effect arising from different orbital velocities at slightly different Galactocentric distances. In this scenario, the Perseus complex kinematics is governed by the Galactic potential, possibly perturbed by the Perseus spiral arm, rather than internal dynamical processes.

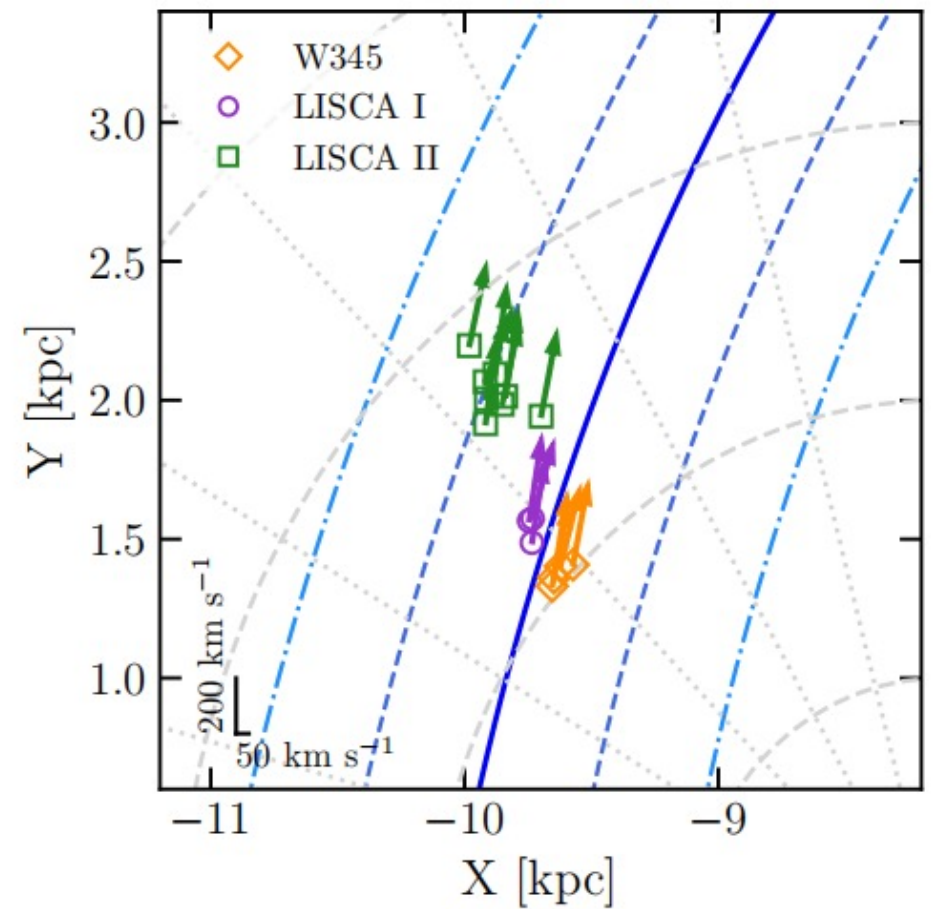


**Fig. 11.** XY projection of the star cluster Galactocentric positions, while arrows show the  $V_X$ ,  $V_Y$  velocities (with velocity scale reported in the bottom-left corner). Galactocentric coordinates were obtained by direct de-projection of the 6D coordinates listed in Table 4. Each cluster is color-coded according to the structure it belongs, namely orange diamonds for W345, purple circles for LISCA I, and green squares for LISCA II. The blue lines show the Perseus spiral arm model (solid) by Reid et al. (2019), with one time (dashed) and twice (dash-dotted) the arm width. The background grid is a Heliocentric polar grid with the dashed gray lines showing distances from 1 to 4 kpc, and the dotted ones sampling the angular direction every 15 degrees.

# Orbits in an axisymmetric potential

- i) LISCA I clusters move slightly outward in the Galactic plane, and toward LISCA II ;
- ii) Berkeley 65 and NGC 869, depart the most from the other neighbor clusters. This is likely due to the difference in their vLOS to the other clusters;
- iii) Going back in time in the cluster orbit reconstruction, LISCA I appears to converge toward the W345 complex.
- iv) LISCA II and W345 are in fact approaching each other.
- v) They do not observe a Hubble-like expansion of the region as suggested by RománZúñiga et al. (2019). According to their reported rate, in 150 Myr the region should reach a size of about 5 kpc, inconsistent with

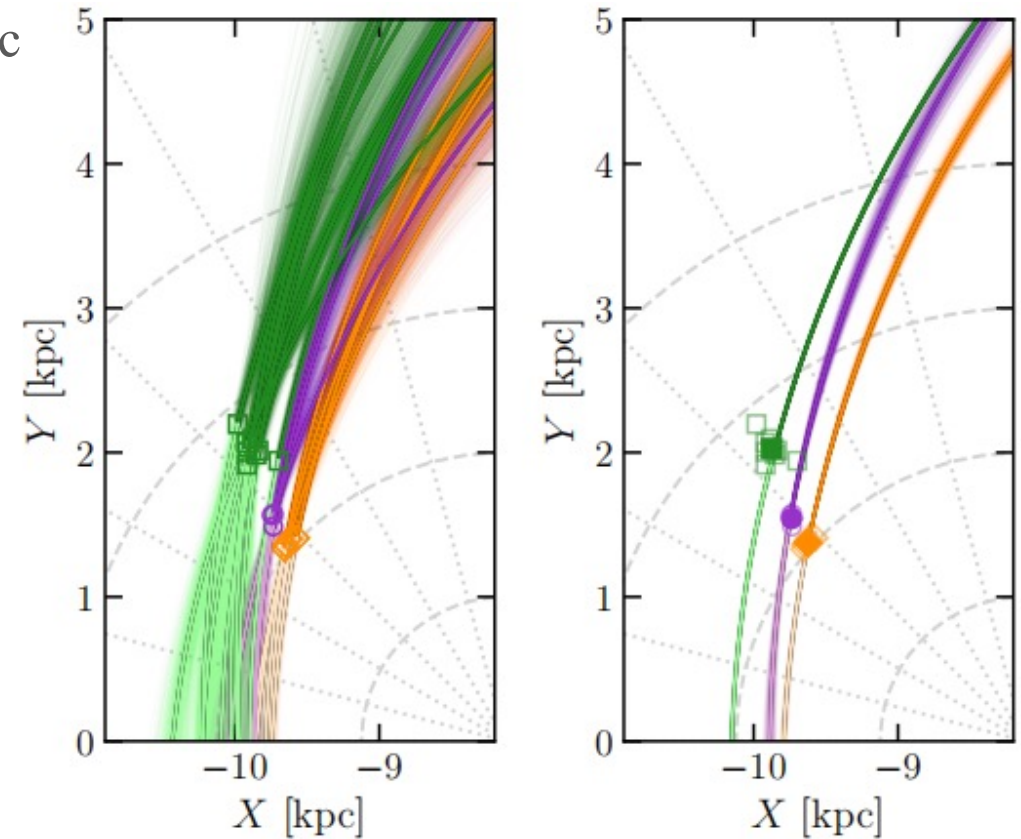


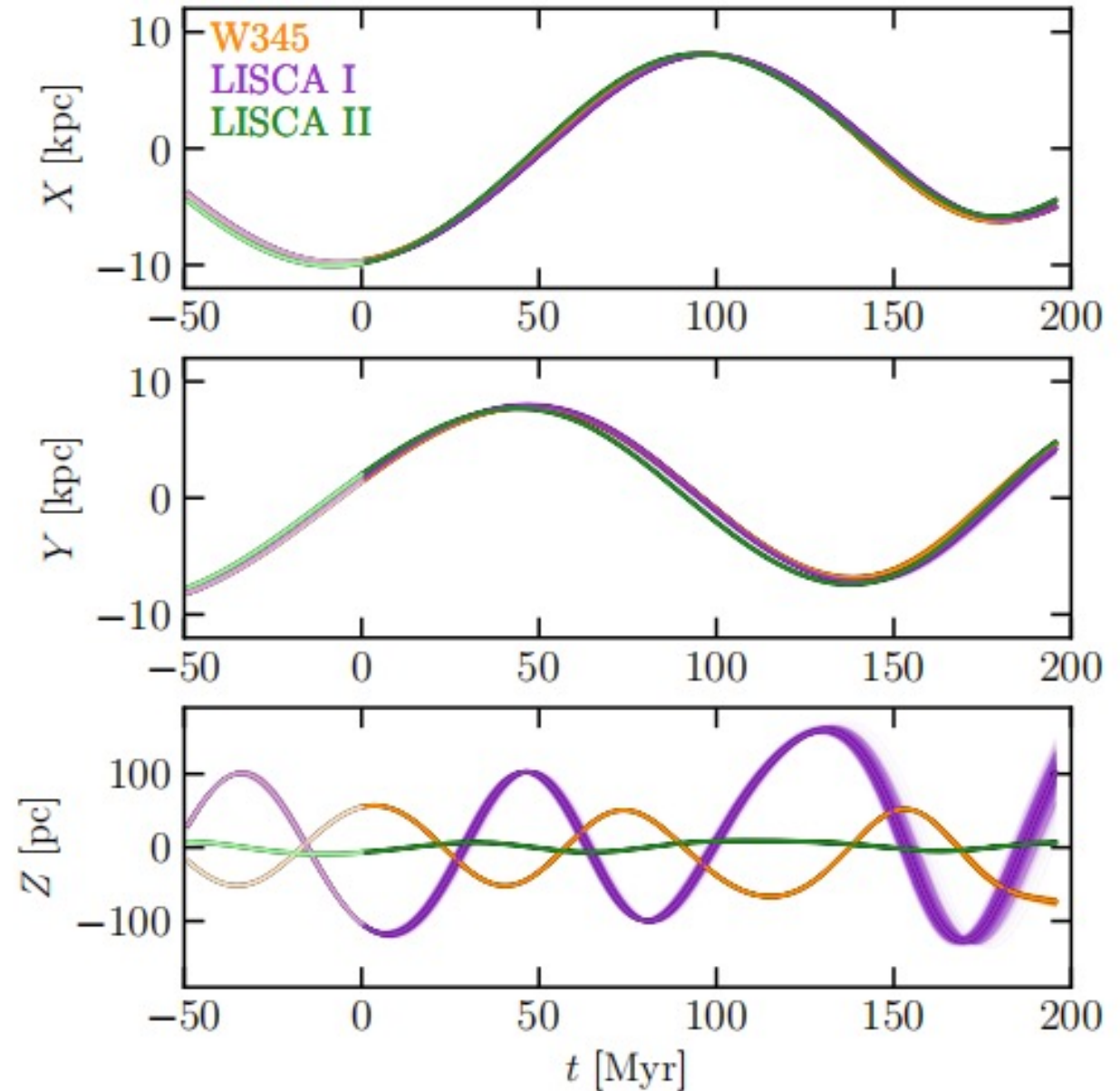
**Fig. 12.** XY projection for individual cluster orbits (left panel) and stellar cluster aggregates (right panel). Darker lines trace the orbits forward in time, whereas lighter ones are backward. Thin lines show orbit integrations from multiple initial condition extractions while thicker ones show median orbits. Present-day cluster positions are also marked: orange diamonds for W345, purple circles for LISCA I, and green squares for LISCA II clusters.

# Orbits in a spiral-perturbed potential

- Spiral structures (see Lin & Shu 1964; Shu 2016; Sellwood & Carlberg 1984, for different formation theories) are believed to play an important role in gathering gas, triggering star formation, and perturbing stellar orbits thanks to the locally deeper potential well (Baba et al. 2016; Tchernyshyov et al. 2018).

# Orbits in a spiral-perturbed potential

- They computed the cluster aggregate orbits to study the evolution of the Perseus complex in the presence of spiral-arm perturbation.
- Figure 16 presents the evolution of Galactocentric coordinates with time. They broadly found that the Perseus spiral arm pulls star clusters towards higher-density regions during their orbit. Since the star clusters in the Perseus complex are within the spiral arm, the stronger gravitational force may keep the star clusters closer for large times when compared to the axisymmetric case.



# Summary and conclusions

- In summary, this study presented a detailed characterization of the Perseus complex, starting from the clusters in the W345 region up to its kinematics on large scales by progressively zooming out. Particular attention was paid to complementing the numerous previous literature studies with kinematic data from Gaia DR3. They showed indeed that kinematics (supplemented by photometric and spectroscopic data) is key to understanding the formation and evolution of large stellar complexes from cluster scales to Galactic ones.

**Thanks**